Edge enhancement through scattering media enabled by optical wavefront shaping

ZIHAO LI[1,2,5 ǂ], ZHIPENG YU[1,2,ǂ], HUI HUI[3,ǂ], HUANHAO LI,[1,2] TIANTING ZHONG[1,2], HONGLIN LIU[4], AND PUXIANG LAI[1,2 *]

[1]Deparment of Biomedical Engineering, The Hong Kong Polytechnic University, Hong Kong SAR, China
[2]The Hong Kong Polytechnic University Shenzhen Research Institute, Shenzhen, China
[3]CAS Key Laboratory of Molecular Imaging, Institute of Automation, Chinese Academy of Sciences, Beijing 100190, China
[4]Key Laboratory for Quantum Optics, Shanghai Institute of Optics and Fine Mechanics, Chinese Academy of Sciences, Shanghai 201800, China
[5]Currently with the Department of Bioengineering, University of Pennsylvania, Philadelphia, PA 19104, USA
ǂThese authors contributed equally to the work
**Corresponding author: puxiang.lai@polyu.edu.hk*

Abstract: Edge enhancement is a fundamental and important topic in imaging and imaging processing, as perception of edge is one of the keys to identify and comprehend the contents of an image. Edge enhancement can be performed in many ways, through hardware or computation. Existing methods, however, have been limited in free space or clear media for optical applications; in scattering media such as biological tissue, light is multiply scattered and information is scrambled to a form of seemingly random speckles. Although desired, it is challenging to accomplish edge enhancement in the presence of multiple scattering. In this work, we introduce an implementation of optical wavefront shaping to achieve efficient edge enhancement through scattering media by a two-step operation. The first step is to acquire a hologram after the scattering medium, where information of the edge region is accurately encoded, while that of non-edge region is intentionally encoded with inadequate accuracy. The second step is to decode the edge information by time-reversing the scattered light. The capability is demonstrated experimentally, and furtherly the performance, as measured by the edge enhancement index (*EI*) and enhancement-to-noise ratio (*ENR*), can be controlled easily through tuning the beam ratio. *EI* and *ENR* can be reinforced by ~8.5 and ~263 folds, respectively. To the best of our knowledge, this is the first demonstration that edge information of a spatial pattern can be extracted through strong turbidity, which can potentially enrich the comprehension of actual images obtained from complex environment.

1. Introduction

Edge enhancement is uniquely important as perception of edge is a key factor for human visual system to identify or comprehend the contents of an image. It has vital roles in broad applications, such as increasing discrimination capacity in pattern recognition [1], detecting dislocation of crystal in biological cells [2], identifying lesion boundaries of cancer [3-6]. The realization of edge enhancement can be traced back to Zernike's seminal work [7], where phase or intensity gradient of an object is enhanced for conspicuity strengthening and tiny-feature detection. Nowadays, edge enhancement can be accomplished digitally through signal processing methods, such as spatial differentiation [8], wavelet transform [9], and Hilbert transform [10], or through physical settings. One well-known example is spiral phase contrast (SPC) imaging, where a spiral phase plate with a topological charge $l = 1$ is placed in the Fourier plane of a 4*f* system [11-13]. Due to the peculiar symmetry of spiral phase, gradients of phase and intensity profile can be isotropically enhanced. SPC method was later extended for microscopy to make image brightness and contrast be significantly better than conventional versions [14]. Another strategy is to employ photorefractive effect to highlight the edge information of an intensity pattern [15-17]. Responding to interferogram, photorefractive materials, governed by the four-wave-mixing mechanism [15], form volumetric optical grating with different local diffraction efficiencies. Manipulating such grating may maximize the diffraction efficiency for edges only while minimize that for other parts; consequentially boundaries of the pattern are enhanced [15]. In addition, some physical filters, such as Laguerre–Gaussian spatial filter [18] and Airy spiral phase filter [19], are also developed to achieve high contrast edge enhancement.

Whilst promising, all filters mentioned above, no matter digital or physical, can only perform edge detection in free space or process signals obtained with ballistic or quasi-ballistic light. These approaches are not able or have not been verified to be compatible with strong scattering media (e.g., ~1 mm beneath human skin [20]), when photons are multiply scattered and optical information is completely disordered [21]. Therefore, existing edge enhancement methods encounter the same trade-off between penetration depth and resolution as all other biomedical optical techniques [22]. High-resolution edge information processing and retrieval at depths in scattering media has been desired in many optical applications yet remains unexplored.

This study aims to tackle this challenge from the perspective of optical wavefront shaping, a relatively new field conceived to manipulate scattered light beyond the diffusion limit [23-27]. Optical phase conjugation (OPC) [24, 27-29] is an example of wavefront shaping that exploits the bilateral nature of light trajectory to "time-reverse" scattered light [30]. The execution of OPC requires an analog [27, 31] or digital [28, 29, 32, 33] phase conjugation mirror (PCM) that firstly holographically records the phase profile of scattered light and secondly projects its phase-conjugated copy back to the medium. As a result, intensity profile of the original incident light field before being scattered can be reconstructed. The whole procedure can be accomplished with two or three steps [33], achieving light manipulation through turbidity as rapidly as a few milliseconds [34, 35]. While related, such a capability thus far has not yet been extended for edge enhancement through scattering media. In this study, we take inspiration from the classic photorefractive approach for edge enhancement in free space [15], and develop a digital optical phase conjugation (DOPC) setup to achieve robust and tunable time-reversed speckle suppression and edge enhancement through thick scattering media by a two-step procedure. First, a hologram that accurately encodes the information of edge only is recorded. Secondly, the edge pattern is selectively decoded by phase conjugating the scattered light. The proposed method is demonstrated experimentally with scalable edge enhancement performance out of seemingly random speckle patterns. Although a lot need to be furthered, this work potentially can be of instructive significance to the processing, comprehension, and analysis of optical images with the presence of scattering.

2. Methods

2.1 Experimental setup

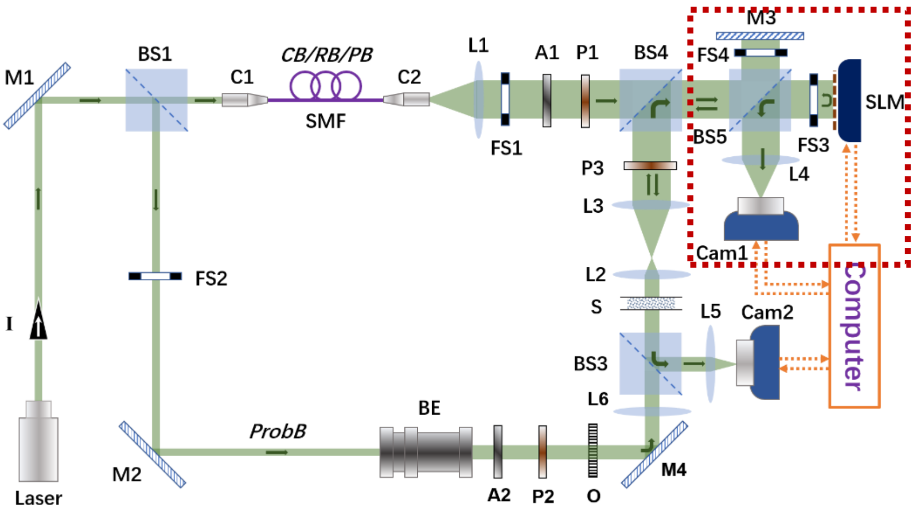

Fig. 1. System setup of DOPC. $A_{1\text{-}2}$: Neutral-density attenuator; BE: Collimated beam expander; $BS_{1\text{-}5}$: Beam splitter cube; $C_{1\text{-}2}$: Optical fiber collimator; Cam_1: Scientific complementary metal–oxide–semiconductor (sCMOS) camera; Cam_2: CMOS camera; $FS_{1\text{-}4}$: Fast shutter; I: Isolator; $L_{1\text{-}3,\,5,\,6}$: Best-form lens; L_4: Camera lens; Laser: CW laser, λ = 532 nm;. $M_{1\text{-}4}$: Mirror; O: Object, a 1951 USAF resolution test chart; $P_{1\text{-}3}$: Linear polarizer; S: Scattering medium; SLM: Phase-only spatial light modulator; SMF: Single-mode optical fiber; CB/RB/PB: Calibration/Reference/ Playback beam; ProbB: Probe beam. Red dash line indicates the module of digital phase conjugation mirror (PCM).

The configuration of DOPC system is presented in Fig. 1. A CW laser source (EXLSR-532–200-CDRH, SPECTRA PHYSICS, coherence length = 300 m) emits a laser beam (λ = 532 nm) which is split by a beam splitter cube (BS_1) into two arms. One is probe beam, and the other is multi-functional beam (calibration/reference/playback beam). The probe beam is expanded by a collimated beam expander and its intensity profile is shaped by a 1951 USAF resolution test chart (Edmund Optics Inc.). The image of the resolution test chart is relayed onto the interior surface of a diffuser (600 grit polished, Thorlabs Inc) by L_6. On the other side, the multi-functional beam is spatially shaped by a single-mode fiber (HP-532, Thorlabs, 1 meter long) to mimic a quasi-ideal point source at the exit of the collimator (C_2). The beam is expanded by a best-form lens (L_1) before entering the digital PCM module. At the beam splitter cube (BS_4), the probe beam and the multipurpose beam merge and are relayed together to the digital PCM, which is configurated by the combination of a scientific CMOS camera (sCMOS, pco.edge 5.5, PCO, pixel size: 6.5×6.5 μm) and a phase-only spatial light modulator (SLM, PLUTO-VIS-056, HOLOEYE). The SLM and the sCMOS camera are pixel-to-pixel conjugated to each other, with a misalignment error less than one pixel. The diffused light pattern right after the diffuser is imaged on the plane of SLM through a 4*f* system configured by L_2 and L_3, where the diffuser and the plane of SLM is spatially quasi-conjugated with each other. The digital PCM has two main purposes, hologram recording and playback, which are respectively accomplished by the sCMOS camera and the phase-only SLM. To observe the playback wavefront, another CMOS camera (Cam_2, pixel size: 2.5×2.5 μm) and L_5 are employed to image the reconstructed intensity distribution of the playback beam after transmitting through the turbid sample. Polarizations and intensities of the probe beam and the multipurpose beam are adjusted by two linear polarizers (P_1 and P_2) and neutral-density attenuators (A_1 and A_2), respectively. Four fast shutters

($FS_{1\text{-}4}$) are equipped to control the ON or OFF state of light beams. Detailed procedures of DOPC operation can be referred to [32, 33].

2.2 Principles of DOPC-based edge enhancement through scattering media

A former study has demonstrated how edges of a binary pattern can be enhanced in free space via photorefractive effect with a piece of $BaTiO_3$ photorefractive crystal [15]. The method proposed in this work is actually a digital analogue of the aforementioned photorefractive edge enhancer. Functions of the photorefractive crystal are provided by a digital PCM, a spatially conjugated camera-SLM module, as enclosed by the red dash line in Fig. 1. On one hand, holographic information is recorded digitally using a digital camera (Cam_1, Fig. 1); on the other hand, a SLM is able to create variable phase profiles, mimicking the effect of grating with variable diffraction efficiency in the crystal.

Starting with hologram recording, the working principles of DOPC-based edge enhancement can be explained as below. The hologram recorded by Cam_1 can be written as

$$I_h = I_{ref} + I_{prob} + 2cos(\varphi)\sqrt{I_{ref} * I_{prob}} \quad (1)$$

where I_h, I_{ref} and I_{prob} denote the intensity of hologram, the reference beam, and the probe beam, respectively; φ is the phase difference between the reference beam and the probe beam. The local modulation efficiency ($M.E.$) of PCM, determined by contrast of the hologram recorded by Cam_1, can be expressed as

$$M.E. = \frac{I_h}{I_{ref} + I_{prob}} = 1 + MD * cos(\varphi) \quad (2)$$

It can be seen that local $M.E.$ of PCM is dominated by the modulation depth ($MD = \frac{2\sqrt{I_{prob} * I_{ref}}}{I_{prob} + I_{ref}}$) [15]. This term can be expressed as a function of the intensity ratio of the probe and reference beams, i.e. $r = \frac{I_{prob}}{I_{ref}}$. So that, $MD(r) = \frac{2\sqrt{r}}{1+r}$. As a result, $M.E.$ can be written as $M.E. = 1 + MD(r) * \cos\varphi$. Considering the one-dimensional situation as following without scattering media:

$$I_{ref}(x) = a \text{ (for all } x\text{)}; \; I_{prob}(x) = \begin{cases} 0 & x \leq -m/2 \\ b & -m/2 < x < m/2 \\ 0 & x \geq m/2 \end{cases} \quad (3)$$

where a, b and m are three finite constants. It represents a simple case of hologram written to Cam_1, where the reference beam is of uniform intensity while the probe beam is of a binary intensity profile, i.e. a box function with a width of m, symmetrical with respect to the origin. But there is an extreme condition for this situation, that is the intensity of the probe beam is considerably larger than that of the reference beam i.e. $a \ll b$. For the dark region of the probe beam ($x < -\frac{m}{2}$ or $x > \frac{m}{2}$), $r = 0$, which leads to $MD(r) = 0$. For the bright region of probe beam ($-\frac{m}{2} < x < \frac{m}{2}$), $r = \frac{b}{a}$, being considerably large, which also yields $MD(r) \approx 0$. The situation is different, however, for the edges ($x = -\frac{m}{2}$ or $x = \frac{m}{2}$). It is considered to exist a transition status where $I_{ref}(x) \sim I_{prob}(x)$, making the *in situ* $MD(r)$ maximum that equals to unity [15].

In the existence of the scattering media, the scattering light field recorded by Cam_1 can be expressed by:

$$E_{out} = TE_{in} \tag{4}$$

where E_{in} is the light field of probe beam before the scattering medium, and T is the transmission matrix of the scattering medium. Due to the scattering, the spatial pattern gets completely chaotic and, as a result, edge profile cannot be seen in the disordered optical field. Specifically, the spatial pattern evolves as random speckle pattern when light propagates through the scattering medium in the hologram recording stage. Thus, the original spatial information is encoded in the recorded random speckle pattern; the recorded speckle pattern carries information of the original incident spatial pattern and the scattering medium. Therefore, signal input to the PCM is the fused information of TE_{in}. Due to the phase-conjugated nature, the PCM turns the input into its phase-conjugated copy, $[TE_{in}]^*$.In the hologram playback stage, the light filed (E_{PB}) out of the scattering medium is recorded by Cam_2, which can be written as

$$E_{PB}=(T)^t[TE_{in}]^*=[(T)^+TE_{in}]^* \tag{5}$$

where * denotes complex conjugate while ^{t} and $^+$ respectively signify transpose and conjugate transpose.

A further justification why the time reversal identity of DOPC is able to overcome the scattering and achieve edge enhancement simultaneously is briefed below. In the phase recording stage, Cam_1 records an interferogram formed by the reference beam (E_{ref}) and the scattered probe beam (TE_{in}). After the scattering medium, the probe beam is scrambled. In the playback section, the output light field ($(T)^+(T)E_{in}$) from the scattering medium appears even more scrambled. But, within a time-invariant system, one can assume that $(T)^+(T) \approx I$, where I denotes an identity matrix. That is, the output light is exactly conjugated to the probe beam. Therefore, the time-reversal playback essentially decodes the original pattern from a seemingly random speckle pattern by reciprocating the transmission matrix, enabling scattering suppression at the front side of the scattering medium.

For DOPC systems, a Camera-SLM module is employed to record the probe-reference interference pattern and retrieve a phase profile to mimic the effect of grating in analogue OPC. Thus, the precision of the retrieved phase (to be loaded on the SLM) matters. In our system, the primary phase retrieval precision is determined by the smallest bit depth of the digital devices (Cam_1: 16 bits; SLM: 8 bits) Through simulation (please refer to the Supplementary), it is found that the calculated phase is most accurate when the two beams of interference are equally intense, and the accuracy is reduced with increased imbalance in beam ratio (Fig. S1). Therefore, in our system, when the beam ratio $r = 1$, the whole object can be recovered with fair fidelity due to the minimum phase error. With increased beam ratio r, for non-edge regions the phase retrieval accuracy drops due to imbalance of interfering beam ratio. But for edges, the precision of calculated phase remains optimum due the existence of transition status where $I_{ref}(x)\sim I_{prob}(x)$. Under this condition ($I_{obj} \gg I_{ref}$), when the SLM is illuminated by the reference beam in the playback stage, the generated conjugated light corresponding to the non-edge regions may deviate from its ideal optical paths. As a result, the non-edge regions are harder to be recovered; more and more photons contribute to the background noise when they propagate through the scattering medium. In comparison, the edge areas are reinforced from the background.

2.3 Quantification of edge enhancement effect

For a characteristic unenhanced edge (Fig. 2a) in an intensity pattern, it can be divided into three portions, ground level (G), brink (B), and upper level (U). In our experiment, the lengths of G and U are both set to be 30 pixels. For an enhanced edge (Fig. 2b), two additional parameters are defined, the summit (S) (maximum pixel intensity) and the valley (V) (minimum pixel intensity) in the regime of brink. To quantify the absolute edge enhancement effect, the concept of edge enhancement-index (EI) is introduced [38, 39]: $EI = \frac{(S-V)/(S+V)}{(\mu_U-\mu_G)/(\mu_U+\mu_G)}$, where μ_U and μ_G are the mean of intensity values of U and G, respectively. For a non-enhanced typical edge, $\mu_U \approx S$, $\mu_G \approx V$ and therefore the edge enhancement index $EI \approx 1$. Larger EI indicates greater absolute edge enhancement effect. However, only EI is not sufficient for quantifying the visual conspicuity of the edge, as the noise level also influences the visual effect (Fig. 2c). Thus, the concept of edge enhancement-to-noise ratio (ENR) is also defined to quantify the edge enhancement effect relative to the noise level [38]: $ENR = \frac{(S-V)}{\sqrt{\sigma_U^2+\sigma_G^2}}$, where σ_U and σ_G are the standard deviation of intensity values of U and G, respectively. Less noise in U and G and greater difference in S and V will lead to larger value of ENR, indicating better visual edge enhancement effect relative to the noise level.

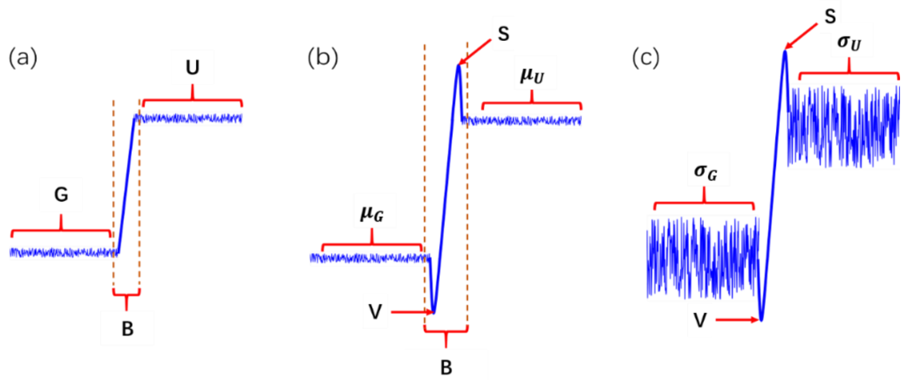

Fig. 2. Anatomy and metrics of an edge. (a) A regular unenhanced edge can be divided into three portions, including ground level (G), brink (B), and upper level (U). The lengths of G and U occupy 30 pixels in our experiment. (b) For an enhanced edge, the maximum and minimum pixel intensity of the portion B are termed as summit (S) and valley (V). To quantify the absolute edge enhancement effect, the concept of edge enhancement-index $EI = \frac{(S-V)/(S+V)}{(\mu_U-\mu_G)/(\mu_U+\mu_G)}$ is introduced, where μ_U and μ_G are mean of intensity values of U and G, respectively. (c) The noise level of an edge influences the visual enhancement effect and thus the concept of edge enhancement-to-noise ratio $ENR = \frac{(S-V)}{\sqrt{\sigma_U^2+\sigma_G^2}}$ is defined, where σ_U and σ_G are standard deviation of the intensity values of U and G, respectively.

---

3. Results and Discussion

With a fine-tuned DOPC system, experiments are conducted to enhance edge of an intensity pattern through strong scattering media. Transmitting through the resolution test chart, the intensity profile of the probe beam is shaped into a pattern "0", carrying the spatial information. This original pattern of interest is recorded by Cam_1, as shown in Fig. 3a. Three horizontal dashed primitive lines with the length of 280 pixels are created in the Fig. 3a and the line charts (b)-(d) correspondingly show the horizontal intensity distributions along these lines. A and B denote the inner and outer rim of the pattern "0", respectively. For edge B, the mean *EI* and *ENR* are calculated as 0.91 and 42.77, respectively. Then, a scattering 600-grit ground glass diffuser (S, Fig. 1) is positioned into the DOPC system. As shown in Fig. 3e, the intensity profile of the probe beam captured by Cam_1 becomes a random speckle pattern after penetrating through the ground glass and no edge profile can be found, indicating that the spatial information of the object has been completely disordered due to scattering. Despite of that, information of the object is encoded within the speckle pattern. Therefore, the next step is to selectively retrieve the edge pattern from this scrambled light field.

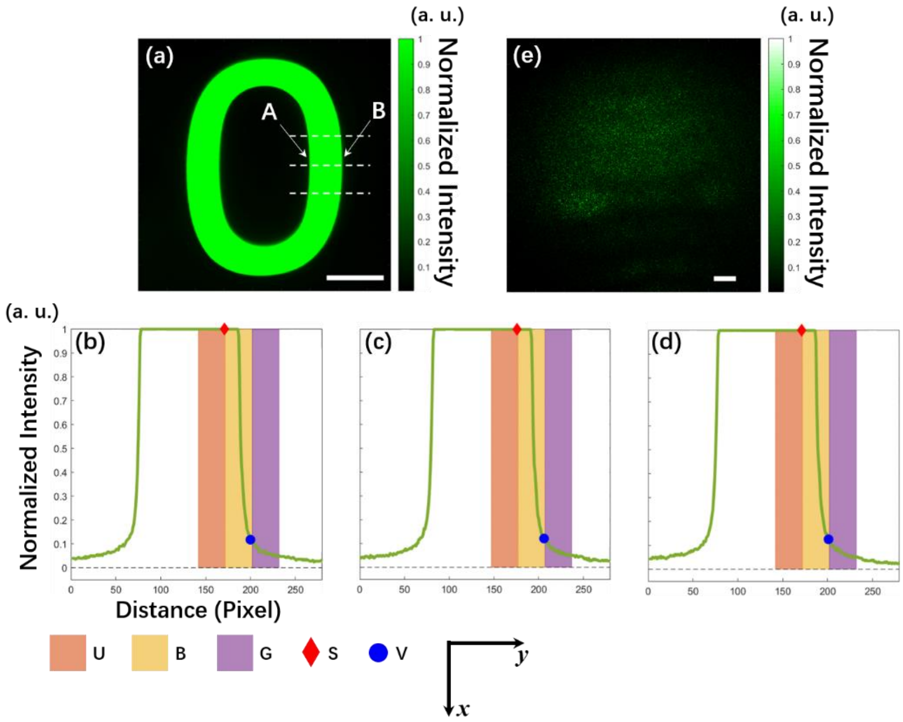

Fig. 3. Intensity profile of the probe beam before and after transmitting through the scattering medium. (a): Intensity profile of the incident probe beam, a quasi-binary pattern of number "0", shaped by the resolution test chart. Three horizontal white dashed primitive lines (1-3) with the length of 280 pixels are created. The intensity distribution along the line 1-3 are respectively shown in (b)-(d). A and B denote the inner and outer rim of the pattern "0", respectively. For edge B, the mean *EI* and *ENR* are calculated as 0.91 and 42.77, correspondingly. U: Upper level; B: Brink; G: Ground level; S: Summit; V: Valley. (e) Intensity profile of the probe beam after penetrating a ground glass diffuser, which is a seemingly random speckle pattern with no obvious edge profile can be found. Scale bar: 500 μm

---

To demonstrate the progressive formation of DOPC-based edge enhancement through scattering media, the intensity ratio ($r = \overline{I_{prob}}/\overline{I_{ref}}$) between the probe and reference beams is carefully adjusted to be 0.02, 0.10, 1.0, 10, and 50, respectively, during the hologram writing. Note that the intensity of the probe beam/speckle pattern ($\overline{I_{prob}}$) is represented by the mean value of all pixels within the region of interest (ROI), e.g. Fig. 3(e), while the intensity of the reference beam ($\overline{I_{ref}}$) is characterized within the same ROI in the same manner.

The intensity patterns of the conjugated light field recorded by Cam_2 in the playback stage are shown in Fig. 4 (the first row). As seen, the edge information can be retrieved well from random speckle patterns through DOPC. That said, there are still quite some residual speckle grains even with the

DOPC compensation. Especially in Fig. 4a and e, speckle grains are not sufficiently suppressed because of inefficient hologram writing due to the small value of *r*. With increased *r* value, intensities of the retrieved non-edge regions are suppressed, but the edges are now selectively highlighted (Fig. 4i, m, and q). To quantify the transition, similar to Fig. 3a, three 280-pixel horizontal dashed lines (1-3) are created for the first row of Fig. 4. The intensity distributions along these lines are respectively plotted in the subfigures in the second, third and fourth rows of Fig. 4, as indicated by the green lines. For example, (b)-(d) are the intensity profiles corresponding to Lines 1-3 in (a), while (f)-(h) correspond to Lines 1-3 in (e). As seen, when *r* is increased, the degree of edge enhancement is boosted due to the robust speckle elimination. When *r* = 50, as shown in Fig. 4r, s and t, the ratio of the noise (speckle grains) to the signal (edges) is strongly suppressed yet the image boundaries are greatly highlighted.

It is also very important to note that whist related, DOPC-based image and edge enhancement through scattering media are essentially two different directions: for regular imaging through scattering media (not aimed for edge enhancement), the optimal performance is usually acquired around *r* = 1, when the $M.E.$ of the PCM achieves maximum at both bright region and edges (but is still zero in the dark region), as confirmed in Fig 4i. It should be clarified that the mean intensity of speckle in the ROI equal to that of reference beam is not necessary to be the optimal intensity ratio for recovering the full image. As seen in Fig. 4i, edges start to protrude when *r* = 1. However, situation of *r* = 1 is the one closest to the optimal image recovery, compared to other four intensity ratios in Fig. 4. If the purpose is to enhance the edge profile only while the other parts of the image are suppressed, a large value of *r* is preferred, i.e., the probe beam should be sufficiently stronger than the reference beam (as in Fig. 4q). Such difference also highlights the motivation of the study as existing knowledges or experiences on optical focusing and imaging through scattering media cannot be directly applied for edge enhancement.

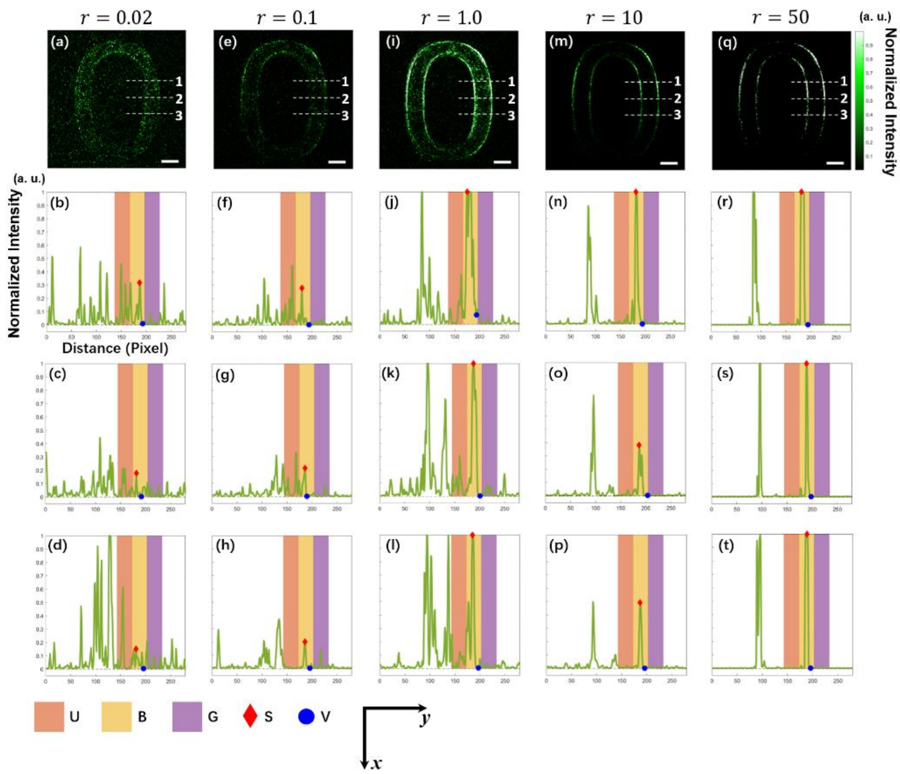

Fig. 4. DOPC-based edge enhancement through scattering media. Five images, (a), (e), (i), (m), (q) are recorded by the CMOS camera (Cam_2 in Fig. 1) in the playback stage. The intensity ratio (r) between the probe and the reference beams is tuned to different values (0.02, 0.10, 1.0, 10, 50) during the hologram writing. Three 280-pixel horizontal dashed lines (1-3) are created for the figures in the first row. The intensity distributions along Lines 1-3 are respectively shown in the figures in the second, third and fourth row, as indicated by the green lines. For example, (b)-(d) are the intensity profiles corresponding to Lines 1-3 in (a), while (f)-(h) correspond to the lines in (e). U: Upper level; B: Brink; G: Ground level; S: Summit; V: Valley. Scale bar: 250 μm.

To further quantify the performance of DOPC-based edge enhancement through turbidity, in Fig. 5 we plot *EI* and *ENR* versus different beam intensity ratios. Each data point represents the mean value of *EI* or *ENR* from calculations of Lines 1-3. The *x*-axis represents the common logarithmic scale of the intensity ratio of between the probe and reference beams, i.e. $lg(r)$. As seen, the mean *EI* (to the left axis) increases from 2.18 (*r*=0.02) to 18.52 (*r*=50), and the mean *ENR* (to the right axis) increases from 2.00 (*r*=0.02) to 525.94 (*r*=50). Even compared to the direct image of the object in free space (Fig. 3a), whose mean *EI* and mean *ENR* are respectively 0.91 and 42.77, the effect of edge enhancement as measured by these two parameters are quite significant, even though a strong scattering medium is penetrated.

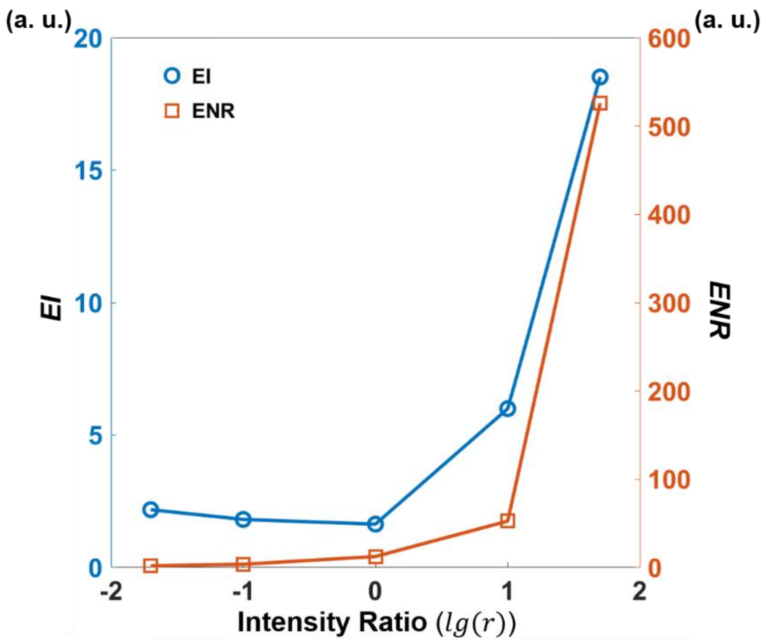

Fig. 5. Edge enhancement-index (*EI)* and edge enhancement-to-noise ratio (*ENR)* of edge B for different values of r (0.02, 0.10, 1.0, 10, 50). The *x*-axis represents the common logarithmic scale of the intensity ratio of between the probe and reference beams, i.e. $lg(r)$. *EI* increases from 2.18 to 18.52, and *ENR* increases from 2.00 to 525.94.

The aforementioned results once again confirm the rationality of the proposed method to enhance object boundary through scattering media. Without wavefront manipulation, optical signals, which is an intensity spatial pattern in this study, are thoroughly disordered when transmitting through scattering media and become seemingly random speckle patterns. In this work, DOPC serves as an effective turbidity suppressor and is able to manipulate the optical wavefronts even through complex media. By tuning the probe-reference beam intensity ratio and hence the local modulation efficiency of the PCM as well as calculated phase precision, DOPC is capable to generate modulated wavefronts so that edge profile can be significantly reinforced from massive speckle noise. That said, we should note the limitation of the performance. Even with a perfect DOPC system, the recovery efficiency is still limited due to the finite control elements of the SLM and other factors such as the uneven spatial distribution of the optical beams and the system calibration imperfection. As a result, only a fraction of speckles is collected and only a fraction of the transmission matrix of the scattering medium is utilized to time reverse the scattered probe beam. Therefore, in practice DOPC is not able to totally overcome scattering, and the recovered edges are still influenced by scattering, as can be observed in Fig. 4.

4. Conclusion

Edge enhancement plays an important role in many aspects of optical imaging and imaging processing. Recent developments in optical wavefront shaping have paved the way to achieve high quality optical focusing and imaging within or through scattering media; edge enhancement through strong turbidity, however, remains unexplored. While related, existing knowledges or experiences cannot be directly applied for edge enhancement through scattering media. In this study, we propose an effective two-step digital optical phase conjugation (DOPC) approach. First, a digital hologram is obtained, where information of the object and the edge is encoded with distinct accuracy (high for edges but low for non-edge regions); second, the edge profile is reinforced by phase conjugating the scattered light while the non-edge regions are significantly suppressed. In experiment, with a 600-grit ground glass diffuser as the scattering medium, our method allows for significant visual enhancement of the edges from noisy speckle patterns. As measured by the enhancement index (*EI*) and enhancement to noise ratio (*ENR*), the edges can be reinforced by ~8.5 and ~263 times, respectively, benefiting from the robust speckle suppression capability. To the best of our knowledge, this is the first time that edge information of a spatial pattern can be extracted clearly through strong turbidity. Moreover, the performance of the edge extraction and enhancement is controllable through tuning the efficiency of the phase conjugation mirror. With further development, this approach may potentially find broad applications or inspire new methods to enrich the comprehension of optical images in the scenario of scattering, such as at depths in biological tissue.

Acknowledgements

The work is financially supported by National Natural Science Foundation of China (81671726), National Key Research and Development Program of China (2016YFC0103803, 2017YFA0700401), National Natural Science Foundation of China (81627805, 81930048, 81671851, and 81827808), Hong Kong Research Grant Council (25204416), Hong Kong Innovation and Technology Commission (ITS/022/18), Shenzhen Science and Technology Innovation Commission (JCYJ20170818104421564), Guangdong Science and Technology Commission (2019A1515011374), and CAS Scientific Instrument R&D Programs (YJKYYQ20170075).

Disclosures

The authors declare no conflicts of interest.

References

1. H. Ge, B. Wang, W. Ji, J. Wei, L. Wang, and Z. Huang, "Photorefractive edge-enhancement and its application to pattern recognition," Proc. SPIE **5280**, 777-784 (2004).
2. A. Jesacher, S. Furhapter, S. Bernet, and M. Ritsch-Marte, "Shadow effects in spiral phase contrast microscopy," Phys. Rev. Lett. **94**, 233902 (2005).
3. P. Nisthula and R. Yadhu, "A novel method to detect bone cancer using image fusion and edge detection," Int. J. Eng. Comp. Sci. **2**, 2012-2018 (2013).
4. F. Qadir, M. Peer, and K. Khan, "Efficient edge detection methods for diagnosis of lung cancer based on two-dimensional cellular automata," Adv. Appl. Sci. Res. **3**, 2050-2058 (2012).
5. M. Diwakar, P. K. Patel, and K. Gupta, "Cellular automata based edge-detection for brain tumor," in 2013 International Conference on Advances in Computing, Communications and Informatics, (IEEE, 2013), pp. 53-59.
6. D. Lu, X.-H. Yu, X. Jin, B. Li, Q. Chen, and J. Zhu, "Neural network based edge detection for automated medical diagnosis," in 2011 IEEE International Conference on Information and Automation, (IEEE, 2011), pp. 343-348.
7. F. Zernike, "Phase contrast, a new method for the microscopic observation of transparent objects," Physica **9**, 686-698 (1942).
8. T. Zhu, Y. Zhou, Y. Lou, H. Ye, M. Qiu, Z. Ruan, and S. Fan, "Plasmonic computing of spatial differentiation," Nat. Commun. **8**, 15391 (2017).
9. A. Grossmann, "Wavelet transforms and edge detection," in *Stochastic processes in physics and engineering,* S. Albeverio, P. Blanchard, M. Hazewinkel, and L. Streit, ed.

(Springer, 1988).

10. K. Kohlmann, "Corner detection in natural images based on the 2-D Hilbert transform," Sig. Process. **48**, 225-234 (1996).

11. M. Ritsch-Marte, "Orbital angular momentum light in microscopy," Phil. Trans. R. Soc. A **375**, 20150437 (2017).

12. X. D. Qiu, F. S. Li, W. H. Zhang, Z. H. Zhu, and L. X. Chen, "Spiral phase contrast imaging in nonlinear optics: seeing phase objects using invisible illumination," Optica **5**, 208-212 (2018).

13. S.-K. Liu, C. Yang, S.-L. Liu, Z.-Y. Zhou, Y. Li, Y.-H. Li, Z.-H. Xu, G.-C. Guo, and B.-S. Shi, "Up-conversion imaging processing with field-of-view and edge enhancement," Phys. Rev. Appl. **11**, 044013 (2019).

14. S. Fürhapter, A. Jesacher, S. Bernet, and M. Ritsch-Marte, "Spiral phase contrast imaging in microscopy," Opt. Express **13**, 689-694 (2005).

15. J. Feinberg, "Real-time edge enhancement using the photorefractive effect," Opt. Lett. **5**, 330-332 (1980).

16. J. Huignard and J. Herriau, "Real-time coherent object edge reconstruction with Bi 12 SiO 20 crystals," Appl. Opt. **17**, 2671-2672 (1978).

17. J. O. White and A. Yariv, "Real-time image processing via four-wave mixing in a photorefractive medium," in *Landmark Papers On Photorefractive Nonlinear Optics,* P. Yeh and C. Gu, ed. (World Scientific, 1995).

18. C.-S. Guo, Y.-J. Han, J.-B. Xu, and J. Ding, "Radial Hilbert transform with Laguerre-Gaussian spatial filters," Opt. Lett. **31**, 1394-1396 (2006).

19. Y. Zhou, S. Feng, S. Nie, J. Ma, and C. Yuan, "Image edge enhancement using Airy spiral phase filter," Opt. Express **24**, 25258-25268 (2016).

20. L. V. Wang and H.-i. Wu, *Biomedical optics: principles and imaging* (John Wiley & Sons, 2012).

21. J. W. Goodman, *Speckle phenomena in optics: theory and applications* (Roberts and Company Publishers, 2007).

22. Z. Ding, H. Ren, Y. Zhao, J. S. Nelson, and Z. Chen, "High-resolution optical coherence tomography over a large depth range with an axicon lens," Opt. Lett. **27**, 243-245 (2002).

23. P. Lai, X. Xu, H. Liu, Y. Suzuki, and L. V. Wang, "Reflection-mode time-reversed ultrasonically encoded optical focusing into turbid media," J. Biomed. Opt. **16**, 080505 (2011).

24. Y. Liu, P. Lai, C. Ma, X. Xu, A. A. Grabar, and L. V. Wang, "Optical focusing deep inside dynamic scattering media with near-infrared time-reversed ultrasonically encoded (TRUE) light," Nat. Commun. **6**, 5904 (2015).

25. C. Ma, F. Zhou, Y. Liu, and L. V. Wang, "Single-exposure optical focusing inside scattering media using binarized time-reversed adapted perturbation," Optica **2**, 869-876 (2015).

26. I. M. Vellekoop and A. Mosk, "Focusing coherent light through opaque strongly scattering media," Opt. Lett. **32**, 2309-2311 (2007).

27. Z. Yaqoob, D. Psaltis, M. S. Feld, and C. Yang, "Optical phase conjugation for turbidity suppression in biological samples," Nat. Photonics **2**, 110-115 (2008).

28. I. M. Vellekoop, M. Cui, and C. Yang, "Digital optical phase conjugation of fluorescence in turbid tissue," Appl. Phys. Lett. **101**, 081108 (2012).

29. K. Si, R. Fiolka, and M. Cui, "Fluorescence imaging beyond the ballistic regime by ultrasound-pulse-guided digital phase conjugation," Nat. Photonics **6**, 657-661 (2012).

30. J.-H. Park, Z. Yu, K. Lee, P. Lai, and Y. Park, "Perspective: Wavefront shaping techniques for controlling multiple light scattering in biological tissues: Toward in vivo applications," APL Photonics **3**, 100901 (2018).

31. H. Liu, X. Xu, P. Lai, and L. V. Wang, "Time-reversed ultrasonically encoded optical focusing into tissue-mimicking media with thickness up to 70 mean free paths," J. Biomed. Opt. **16**, 086009 (2011).

32. Z. Yu, M. Xia, H. Li, T. Zhong, F. Zhao, H. Deng, Z. Li, D. Li, D. Wang, and P. Lai, "Implementation of digital optical phase conjugation with embedded calibration and phase rectification," Sci. Rep. **9**, 1537 (2019).

33. Z. Yu, J. Huangfu, F. Zhao, M. Xia, X. Wu, X. Niu, D. Li, P. Lai, and D. Wang, "Time-reversed magnetically controlled perturbation (TRMCP) optical focusing inside scattering media," Sci. Rep. **8**, 2927 (2018).

34. Y. Liu, C. Ma, Y. Shen, J. Shi, and L. V. Wang, "Focusing light inside dynamic scattering media with millisecond digital optical phase conjugation," Optica **4**, 280-288 (2017).

35. D. Wang, E. H. Zhou, J. Brake, H. Ruan, M. Jang, and C. Yang, "Focusing through dynamic tissue with millisecond digital optical phase conjugation," Optica **2**, 728-735 (2015).

36. S. Popoff, G. Lerosey, R. Carminati, M. Fink, A. Boccara, and S. Gigan, "Measuring

the transmission matrix in optics: an approach to the study and control of light propagation in disordered media," Phys. Rev. Lett. **104**, 100601 (2010).

37. C. Ma, X. Xu, Y. Liu, and L. V. Wang, "Time-reversed adapted-perturbation (TRAP) optical focusing onto dynamic objects inside scattering media," Nat. Photonics **8**, 931-936 (2014).

38. E. F. Donnelly, R. R. Price, and D. R. Pickens, "Quantification of the effect of system and object parameters on edge enhancement in phase-contrast radiography," Med. Phys. **30**, 2888-2896 (2003).

39. E. F. Donnelly and R. R. Price, "Quantification of the effect of kVp on edge-enhancement index in phase-contrast radiography," Med. Phys. **29**, 999-1002 (2002).